The International Journal of Advanced Manufacturing Technology
https://doi.org/10.1007/s00170-019-03582-9

ORIGINAL ARTICLE

Atomistic simulation of diffusion bonding of dissimilar materials undergoing ultrasonic welding

Avik Samanta[1] · Shaoping Xiao[1] · Ninggang Shen[2] · Jingjing Li[3] · Hongtao Ding[1]

Received: 18 December 2018 / Accepted: 11 March 2019

Abstract
Ultrasonic welding (UW) process offers the ability to create highly efficient solid-state joints for lightweight metal alloys with low power consumption. During the process, a distinct diffusion layer is observed at the joint interface that undergoes severe plastic deformation at elevated temperature. A hierarchical multiscale method is proposed in this study to predict the diffusion behavior of the UW process of dissimilar materials. The method combines molecular dynamics and classical diffusion theory to calculate the thickness of the diffusion layer at the welded interface. A molecular dynamics model is developed for the first time that considers the effect of transverse ultrasonic vibration to simulate the evolution of the diffusion layer. The effect of ultrasonic vibration at the atomic level is assumed to provide thermal energy at the joint interface and the mechanical movement of atoms. The influence of sinusoidal velocity change during ultrasonic vibration is incorporated by numerically time integrating the diffusivity at different ultrasonic velocity. The simulation result shows that the solid-state diffusivity depends on temperature, pressure, and transverse ultrasonic velocity. Higher temperature, pressure, and ultrasonic velocity result in higher diffusivity leading to larger diffusion layer thickness. This article provides a comprehensive review of the diffusion bonding behavior and its dependence on process variables. It also presents a numerical approach combining molecular dynamics and hierarchical multiscale calculation to predict the diffusion layer thickness for the UW process of dissimilar materials.

Keywords Molecular dynamics · Diffusion bonding · Ultrasonic welding · Dissimilar materials · Interface · EAM potential

1 Introduction

Structures made of multi-metal alloys, including aluminum (Al), copper (Cu), magnesium (Mg), nickel (Ni), and titanium (Ti) alloys, are of increasing demand in aerospace, battery for electric vehicles, and electronics industries due to their technical and economic advantages [1]. Solid-state joining mechanism of those dissimilar materials is complex and includes mechanical, chemical, and thermal transformations during the process [2]. In recent years, ultrasonic welding (UW) [3, 4] has become one of the popular choices for solid-state joining because of its low power consumption, easy automation, and environment friendliness [3]. Particularly, it is used to join thin-layered dissimilar materials for cell terminals and bus bars in lithium-ion batteries, which are widely utilized in consumer electronics, smart grids, and electric vehicles. The mostly used metals and metal alloys in these applications include Al, Cu, and other materials with high electrical and thermally conductivities [5].

Some of the existing researches on the UW process of Al-Cu dissimilar material joining focused on the experimental analysis of process optimization, microstructure evolution, and mechanical strength of joining interface [6, 7]. Zhao et al. [6] conducted experiments to join a single layer of Cu with a single layer of Al in a lap joint configuration using different ultrasonic welding energy. After investigating the effect of welding energy on the interface region of Al-Cu ultrasonic welded joint, they concluded that the strength of the welded joint increased until the welding energy increased to a threshold value, and then the strength started to decrease. They also observed that the failure mode of the welded joint also changed from interface de-bonding to nugget pullout with

✉ Hongtao Ding
hongtao-ding@uiowa.edu

[1] Department of Mechanical Engineering, University of Iowa, Iowa City, IA 52242, USA

[2] Tesla, Sparks, NV 89434, USA

[3] The Harold and Inge Marcus Department of Industrial and Manufacturing Engineering, Penn State University, State College, PA 16802, USA

Published online: 26 March 2019

the increase of welding energy. In addition, various microstructures with different morphologies and properties were observed in the interfacial region based on the work done by Wu and co-workers [7].

Although numerous works have been done to study the bonding mechanisms of the UW process for over decades, the process is still arguably the least understood welding process. Various observations have been reported for the UW process including interdiffusion, recrystallization, plastic deformation, work hardening, contaminant breaking, heat generation due to friction and plastic deformation, and melting [8–12]. Particularly, diffusion bonding has been observed at the interface between copper and aluminum for an extended period of welding time [6, 13–17]. It has been observed that the welding time plays a crucial role in determining the thickness of the interfacial diffusion layer [14]. On the other hand, formation of intermetallic compound (IMC) has been reported as well at the interface during the UW process of dissimilar materials [6, 14, 18]. It shall be noted that no existence of the diffusion layer and IMCs was reported during the UW process of Mg and Ti alloy [19]. Xu et al. [18] reported that the formation of the diffusion layer and IMCs depends on the interface temperature during the UW process. They concluded that if the temperature went beyond the melting temperature of one of the working materials, the probability of IMC formation increased. Excessive high ultrasonic welding energies also increase the possibility of the formation of interfacial IMCs [6]. In conclusion, the formation of IMCs in the interface during the UW process significantly depends on material combination and processing condition.

Overall, most of the existing studies of diffusion bonding during the UW process were based on experimental observations at the macroscale. However, diffusion bonding is an atomistic physical phenomenon, in which atoms of one material diffuse into the crystal structure of another material due to the thermal and pressure condition at the material interface. It has been known that molecular dynamics (MD) is a powerful tool to elucidate physical phenomena at the nanoscale, since it is free of experimental uncertainties due to sample preparation, fixture condition, etc. It has been employed to study nanomaterials and composites [20, 21], nanodevices [22, 23], and behavior of lubricant between sliding solids [24]. In the community of advanced manufacturing, MD simulations provided useful information about material nanostructure evolution at the nanoscale during the macroscale manufacturing process like explosive welding, friction stir welding, and metal cutting [25–27]. In one of these works, Chen et al. [25] concluded that the atomic diffusion mostly took place in the unloading state of the explosive welding process based on their MD simulations.

A few MD simulations have been reported to study diffusion bonding at Al-Cu, Cu-silver (Ag), and Ni-molybdenum (Mo) interface [28–31]. Li et al. [28] showed that Cu atoms deeply diffused into Al side, whereas Al atoms hardly diffuse into the interior of the Cu side under atmospheric pressure condition. Chen et al. [29] illustrated that the interface pressure played an important role in determining the diffusion layer thickness of the Cu-Ag joint. It was observed that a higher pressure led to a thicker amorphous interfacial diffusion layer. Chen et al. [30] also studied the effects of temperature and surface roughness on the diffusion joining strength during tensile deformation. One of their observations was that the thickness of the simulated diffusion layer remained similar after it cooled down to room temperature. In addition, Zhang et al. [31] simulated solid-state interfacial reaction in Ni-Mo system and showed amorphization in the interface area. They found that the growth rate of the amorphous layer was higher in the Ni side than the Mo side because Ni had a lower atomic weight. It shall be noted that only thermal loading and pressure at the interface were considered to study diffusion bonding in all of the reported MD simulations. On the contrary, the UW process is significantly different from those reported diffusion bonding processes. During the UW process, ultrasonic vibration is applied parallel to the material top surface. The ultrasonic energy input is one of the prime sources of energy during the process. It has been reported that the vibration amplitude and frequency did not decay significantly from the top layer to bottom layer during the multilayer UW process with fine knurl pattern [32]. Therefore, the transverse velocity loading needs to be considered when studying the diffusion phenomena of the UW process.

The interface diffusion phenomena during the UW process significantly depends on the thermomechanical loading condition at the interface [6, 13–17]. The author's group has previously developed a high-fidelity FE modeling approach using ABAQUS/explicit under 20-kHz vibration [33]. The model considered the high-frequency cyclic loading, thermal softening, and acoustic softening to simulate the dynamic thermomechanical material response at the interface at the continuum scale. The model is capable of providing the dynamic thermomechanical loading during the UW process with shorter welding time. Authors group also developed a DEFORM-based computationally cost-effective model for longer welding time [34]. The effective pressure at the Al-Cu interface, where diffusion occurred, varied from 100 to 150 MPa based on location in the interface [33, 34].

In this paper, a comprehensive study of the diffusion bonding phenomenon during the dissimilar Al-Cu UW process was reported through both experimental observations and numerical analyses. The atomistic bonding phenomena during the UW process are captured for the first time by MD simulations. The novelty in the MD models is that the transverse ultrasonic vibration was considered to mimic the UW process. Since the timescale of the ultrasonic vibration is much higher than the timescale of the MD simulation, several MD simulations are conducted at different positions of the vibration cycle and the

effective diffusivity is calculated by numerical time integration of those positions. Therefore, the effect of ultrasonic vibration on the diffusion bonding during the UW process would be considered. The effects of ultrasonic vibration, pressure, temperature, dissimilar lattice orientation, and crystal defects were studied via MD simulations. In addition, a hierarchical multiscale method, consisting of MD and classical diffusion models, was proposed to predict diffusion layer thickness and compared to the experimental measurements. The outline of this paper is as follows. After the introduction, the methodology of experimental investigation and numerical simulations are described in "Section 2." "Sections 3" includes results and discussion followed by the conclusions.

2 Methodology

2.1 Experimental setup

The UW experiments were carried out with three layers of pure Al sheet (45 mm × 19 mm × 0.2 mm) over a layer of pure Cu sheet (45 mm × 19 mm × 0.5 mm) in a lap joining configuration, as illustrated in Fig. 1. The sheets were joined by a Branson® L20 ultrasonic welder. A clamping force/welding pressure of 0.2 MPa was applied in the vertical direction to hold the joined Al and Cu sheets. The sonotrode was placed on the top of the aluminum sheets to provide ultrasonic vibration in the transverse direction with an amplitude of 35 μm at the 20-kHz frequency. The induced velocity and displacement profiles are shown in Fig. 2. Both of them are sinusoidal curves with a period of 50 μs. The amplitudes are 35 μm and 4.4 m/s respectively for displacement and velocity. They are the maximum displacement and velocity of the sonotrode. During the welding pad (12.7 mm × 8 mm), consisting of 5 × 3 spherical knurls with a radius of 1.2 mm, was inserted under the sonotrode. It has been shown that the vibration amplitude and frequency will not significantly decay when the wave reaches the Al-Cu interface [32]. During the UW process, welding energy of 500 J was used as recommended by Lee et al. [3] to generate a good quality weld.

In addition, real-time temperature monitoring away from the welded zone [35] showed that the temperature in the welded region was in the range of 500 °C~525 °C. Such a temperature is well below the melting temperature of each material and is lower than the eutectic temperature (548.2 °C) of the Al-Cu phase diagram as well. Therefore, melting was less likely to happen for the welding process in this study.

The diffusion bonding interface was characterized between the third Al layer and the Cu layer as shown in Fig. 1. The selected site underwent larger deformation and heat generation as the local welding pressure was higher due to its location at the center beneath the knurl. After welding, focused ion beam (FIB) cut was made at the specified location and scanning transmission electron microscopy (STEM) and energy-dispersive X-ray spectroscopy (EDXS) to get the chemical composition around the Al-Cu interface.

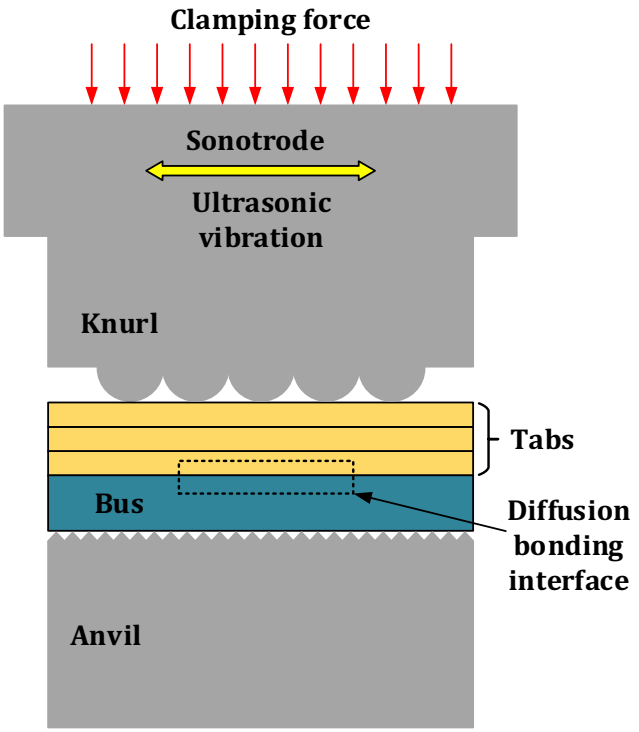

Fig. 1 Schematic representation of the experimental setup for the UW process

2.2 Molecular dynamics

The MD simulations were conducted using a large-scale atomic/molecular massively parallel simulator (LAMMPS) [36] to study the diffusion bonding mechanism during the UW process of dissimilar materials (Al and Cu). Multibody

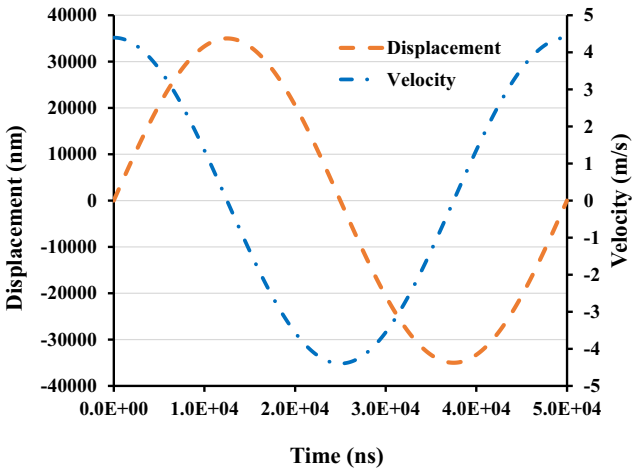

Fig. 2 Ultrasonic displacement and velocity profile during the UW process

embedded-atom method (EAM) potential for Al and Cu [37] was employed to approximate interatomic interactions. During the simulation, the positions, and velocities of the atoms were updated by numerically integrating Newtonian equations of motion. The velocity Verlet algorithm was adopted, and the time step was chosen as 2 fs.

A three-dimensional MD model was developed as shown in Fig. 3. The model consisted of an Al block on the top of a Cu block. The <001> plane was chosen for both materials at the welding interface. The gap between the two blocks was set as the average of the lattice constants of Al (4.05 Å) and Cu (3.615 Å). The lattice sizes of the transverse plane (i.e., *X*-*Y* plane) were chosen to be 28 × 28 and 25 × 25 for Cu and Al respectively so that the Al-Cu mismatch would be as small as 0.03%. Such a misfit at the Al-Cu interface was the same as the experimental setup while the computational cost was manageable.

The heights of Al and Cu blocks were ~25 nm to avoid boundary effects in the vertical direction. Four layers of atoms at the bottom of the Cu block and four layers at the top of the Al block were fixed with applied external pressure as the boundary condition. The periodic boundary condition was applied in transverse directions.

The MD simulation included four stages: relaxing, heating, welding, and cooling. The thermomechanical loading conditions in the interface during the simulation were obtained from the high-fidelity FE model developed by the author's group [33]. At the beginning of the relaxing stage, i.e., relaxation, velocities of atoms were assigned based on the Maxwell-Boltzmann distribution to generate the initial configuration. Then, the MD simulation was conducted in an isothermal-isobaric (NPT) ensemble for at 300 K for 20 ps. The Nose-Hoover thermostat [38, 39] was employed for temperature regulation. In addition, the pressure in the transverse directions was maintained at an atmospheric level using the Nose-Hoover barostat [40], while a pressure of 100 MPa was applied in the vertical direction. The pressure in the vertical direction was simulated using high-fidelity FE model developed by the author's group based on the UW experiment conditions as described in "Section 2.1." After the simulated model reached a thermodynamic equilibrium state, the temperature was increased to 800 K within 200 ps. This heating stage is to imitate that the welding interface was rapidly heated during the UW process. The applied temperature is simulated by macroscale high-fidelity FE calculations [33]. At the stage of welding, the temperature (800 K) was maintained for up to 750 ps, which is assumed as the welding time. The duration of the welding stage in MD simulation was assumed to the welding time, in which the diffusion phenomenon occurs. The pressure conditions in the heating and welding stage were kept as same as the relaxing stage.

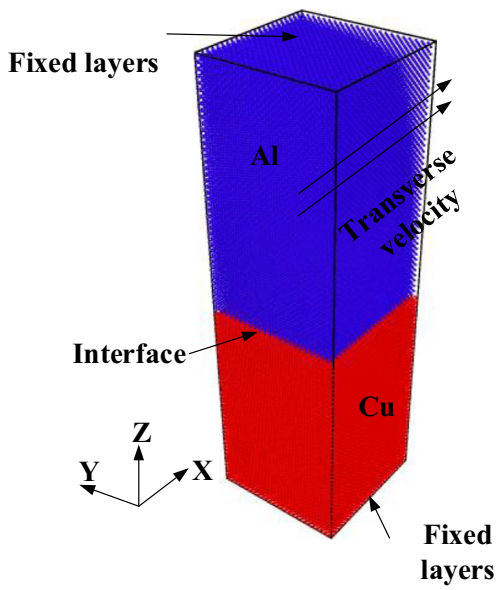

Fig. 3 MD model configuration of the UW process

It shall be noted that the transverse cyclic velocity due to ultrasonic vibration should be applied as boundary condition according to the experimental setup. However, the timescale of MD simulation is a nanosecond, which is far less than the timescale of experiments, i.e., microseconds or seconds. Therefore, the cyclic loading cannot be directly applied in the MD simulations. The loading due to transverse cyclic velocity is decoupled into two separate effects. The first is the induced energy from the ultrasonic vibration and the second is the mechanical movement. The induced energy from ultrasonic vibration was already approximated by increasing the temperature of the simulated system at the stage of heating. To study the effect of relative transverse motion at the Al-Cu interface during the UW process, a transverse velocity was added to each Al atom along one of transverse directions to initiate the relative mechanical movement at the Al-Cu interface. It also needs to keep in mind the velocity direction and magnitude also change during the process. A few simulations were conducted by considering the change of direction and keeping the same magnitude. It was found that the direction change did not have a significant impact on the MD results. To accommodate the change of the magnitude of the transverse velocity from 0 to 4. 4m/s during one-quarter of a vibration cycle, five simulations with different velocity magnitude was considered. Details of the result are discussed in "Section 3." As mentioned earlier, the timescale of the one ultrasonic vibration cycle is much higher than the simulation time of the MD model. To counter this issue, the simulated diffusion results of those five simulations were numerically time integrated to get the equivalent diffusion within a vibration cycle. At the last stage of cooling, the system was cooled down to 300 K for 200 ps, and the diffusion layer thickness was measured based on the molecular configurations after examining the positions of Al and Cu atoms. In MD simulations, 200 ps is enough to gradually reduce the temperature until the simulated

system reaches to a thermodynamic equilibrium state at the room temperature. Such a short time is assigned due to the small size of the MD simulated model as well as the periodic boundary conditions.

2.3 Hierarchical multiscale method

2.3.1 Calculating diffusivity via molecular dynamics

Although MD can elucidate the diffusion phenomena at the nanoscale, it was unable to reproduce the diffusion layer thickness, measured based on STEM images from macroscale experiments, due to the limitation of timescale in MD simulations. A hierarchical multiscale model is proposed in this paper to accurately predict diffusion layer thickness by passing the material diffusivity calculated from MD to the classical diffusion theory which is a continuum model.

It has been known that the material diffusivity at the material interface can be calculated by Fick's first law [41–43], which relates the diffusive flux to the concentration under the assumption of steady state and is given by:

$$J_i = -D_i \frac{\partial \varphi}{\partial x_i} \tag{1}$$

where J_i is the flux of atoms or diffusion flux in direction i, D_i is the diffusion coefficient, i.e., diffusivity, and φ is the atomic concentration. In this study, the diffusion only happens in one direction, so D_i will be used as D in the rest of the article.

Figure 4 schematically represents the molecular model of the Al-Cu diffusion interface. Periodic boundary conditions were applied in all transverse directions while Al and Cu inflow in opposite directions. During the MD simulation, atoms from each side flow inside the diffusion region. Once the simulated system reaches to the thermal dynamic equilibrium state, based on the atomic positions, the diffusion fluxes, J_i (with a unit of atoms/nm^2/ps), of Al and Cu in the diffused region can be determined, as well as the concentration gradient $\left(\frac{\partial \varphi}{\partial z}\right)$. Consequently, the diffusivity of Cu in Al and the diffusivity of Al in Cu can be calculated by Eq. (1) respectively.

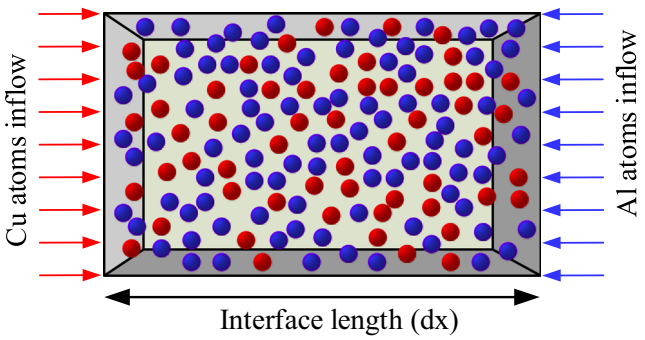

Fig. 4 Schematic MD representation of Fick's first law to calculate the diffusivity at the interface

2.3.2 Predicting the diffusion layer thickness via classical diffusion theory

After passing the diffusivity from the molecular model to the continuum model, the diffusion layer thickness was then calculated via the classical diffusion model. According to the classical diffusion theory, once the system reaches an equilibrium state under the isothermal condition, the regular diffusion process of Cu and Al should meet the classical diffusion equation by Fick's second law [41].

$$\frac{\partial \varphi}{\partial t} = D\nabla^2 \varphi \tag{2}$$

where t is the diffusion time and D is the diffusivity. Since the UW process studied in this paper is a one-dimensional diffusion problem, in which diffusion happens perpendicularly to the contact interface, the conventional solution is as follows:

$$\varphi(z,t) = \frac{N}{2\sqrt{\pi D t}} e^{\left(\frac{-z^2}{4Dt}\right)} \tag{3}$$

where N is the quantity of diffusion matter and z is the diffusion distance. It has been known that integrating the atom concentration function to $3\sqrt{2Dt}$ gives 99.7% accuracy for calculation of the number of diffusion atoms [25], as shown below.

$$\int_0^{3\sqrt{2Dt}} \frac{\varphi(z,t)}{N} dz \approx 99.7\% \tag{4}$$

Thus, the thickness of the diffusion layer (L) can be calculated by:

$$L = \sum_{i=Cu,Al} 3\sqrt{2D_i t} \tag{5}$$

Numerical time integration is performed to calculate the thickness of the diffusion layer.

3 Results and discussions

3.1 Experimental results

EDXS line scanning was performed at a few locations across the Al-Cu interface on a sample produced by the UW process using the experimental condition as described in "Section 2.1." It recorded the elemental composition between two points on either side of the interface along with a straight line. Then, the atomic concentrations of Al and Cu, representing the percentage of material in terms of atom

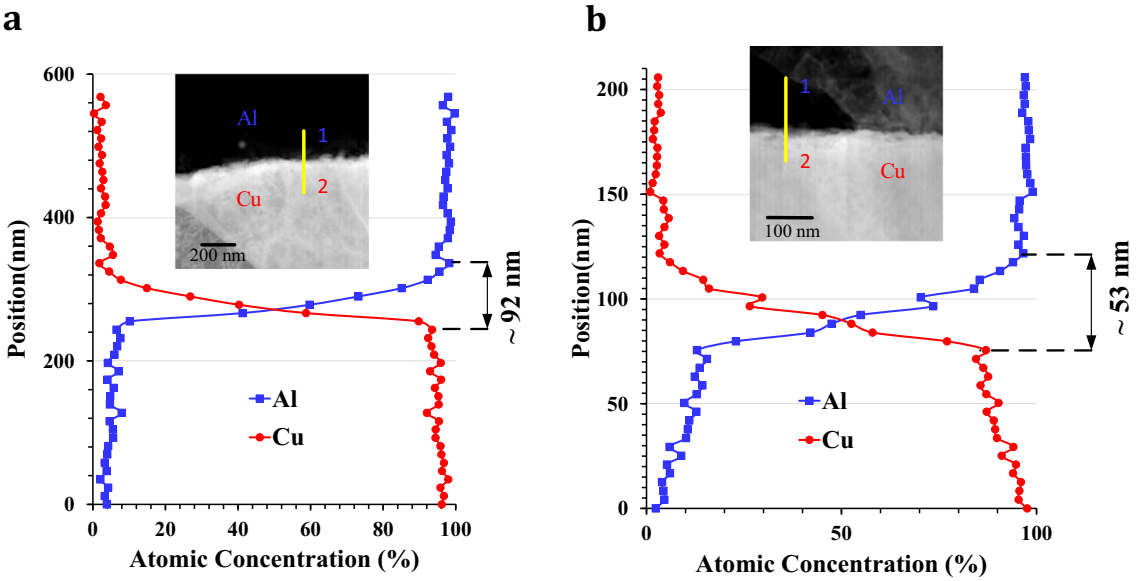

Fig. 5 Material atomic concentration across the weld interface measured by EDXS at two locations. Experimental conditions for the specimen: transverse ultrasonic vibration with a 35-μm amplitude at a 20-kHz frequency, a clamping force/welding pressure of 0.2 MPa

numbers, were calculated and shown in Fig. 5. The corresponding STEM images of the diffusion interface were attached as well. Figure 5 a shows the concentration measurement at one location. The blue dots represent Al while the red dots stand for Cu. The EDXS line scan result shows a smooth transition of elemental concentration from ~0 to 100% for both the element within the diffusion layer. It also shows that no IMC layer was formed at the UW interface. The region, in which the atomic concentrations change, is defined as the diffusion bonding layer. Its thickness was measured as 92 nm. Figure 5 b shows the concentration measurement at the other location, and the diffusion layer thickness was measured as 53 nm. The measured thicknesses at other locations were between 53 and 92 nm. The experimentally measured diffusion layer thickness varies widely along the welding line. Surface roughness difference at various location of the interface and the difference of local stress condition at the peaks and valleys of the knurl pattern contribute to the non-uniformity of the diffusion layer thickness along the welding line.

3.2 MD simulation of diffusion bonding

3.2.1 Diffusion phenomenon

At first, a few MD simulations were conducted to elucidate diffusion phenomenon as described in "Section 2.2." In MD simulations, the interface was heated up to 800 K after relaxation, and the interface pressure was 100 MPa. A transverse velocity of 2.2 m/s was added on each Al atom to initiate the relative motion at the Al-Cu interface. Figure 6 shows the molecular configurations of the diffusion phenomenon after various welding times: 250 ps, 500 ps, and 750 ps. It can be seen that the diffusion layer was thicker under longer welding

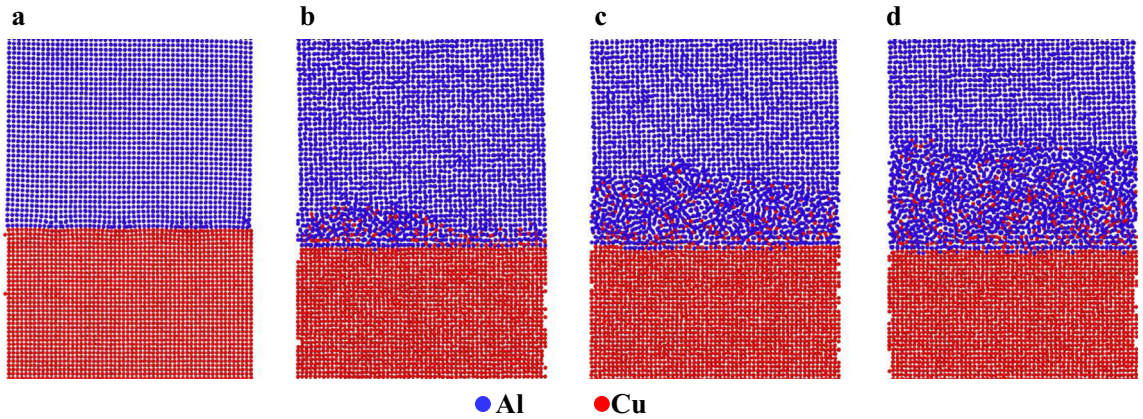

Fig. 6 Molecular configurations of Al-Cu interface: **a** initial configuration after relaxation, **b** after 250 ps, **c** after 500 ps, and **d** after 750 ps

time. In addition, it can be seen that Cu diffused further in Al than Al in Cu.

Figure 7 showed the concentration distribution of Al-Cu when the interface temperature is 800 K. It shows a smooth transition of atom concentration from the Cu layer to the Al layer. It suggests that there is no IMC layer formed in the interface.

3.2.2 Effects of the UW process parameters on diffusion bonding

Using MD simulations, we considered the following effects on diffusion layer thickness: the interface temperature, the interface pressure, and the initial transverse velocity.

Figure 8 shows the evolution of the diffusion layer thickness during the UW process at different interface temperatures: 750 K, 800 K, 850 K, and 900 K. The welding time kept as 750 ps, and the final thickness varied between 6 and 16 nm. It shall be noted that the interface temperature in MD simulations intimates the welding energy utilized in the actual UW process. A higher interface temperature represents higher welding energy. At the same time, high temperature causes the atoms to have thermal vibration with a larger amplitude. As a result, the atoms can diffuse larger depth compared to low temperature.

When considering different interface pressures: 50 MPa, 100 MPa, and 150 MPa, the final diffusion layer thicknesses are different as well, as shown in Fig. 9. The interface pressure assisted the movement of the atoms across the interface. As

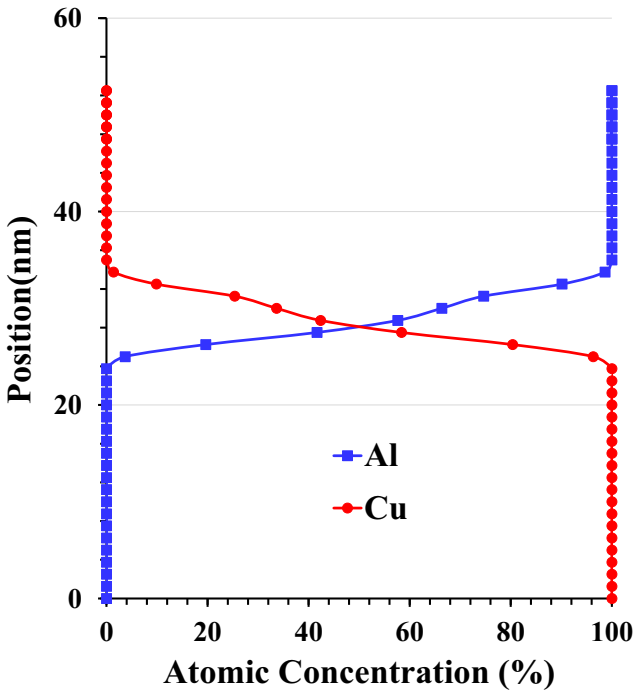

Fig. 7 Concentration distribution in the interface at 800 K

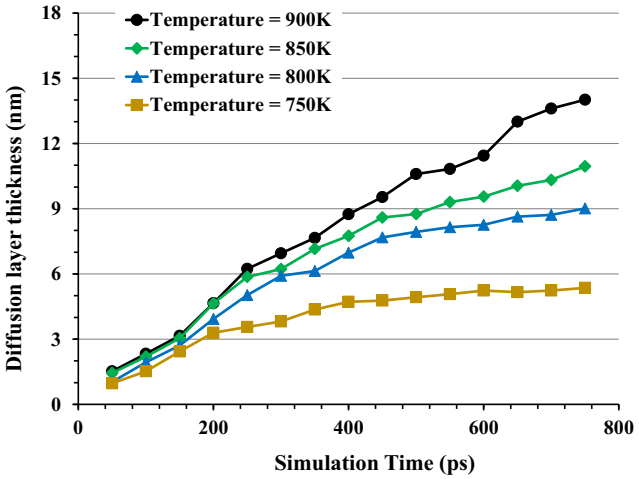

Fig. 8 Thickness of the diffusion layer at different interface temperature

the interface pressure was increased from 50 to 150 MPa, the final thickness was enlarged from 8 to 10 nm.

The application of transverse velocity in the MD model is one of the unique differences from existing molecular simulations of diffusion bonding phenomena. As described in "Section 2.1," after the simulated model was heated to 800 K, a transverse velocity was added to each Al atom to initiate the mechanical relative motion at the Al-Cu interface due to ultrasonic vibration. We first conducted a few simulations by applying a transverse velocity of 2.2 m/s but considering various directions and direction change. At first, two separate simulations were conducted with the transverse velocity applied in opposite directions. The diffusion layer thicknesses were observed very close to each other.

We did observe that the diffusion layer thickness changed if different initial transverse velocities were applied as shown in Fig. 10. When the transverse velocity due to ultrasonic

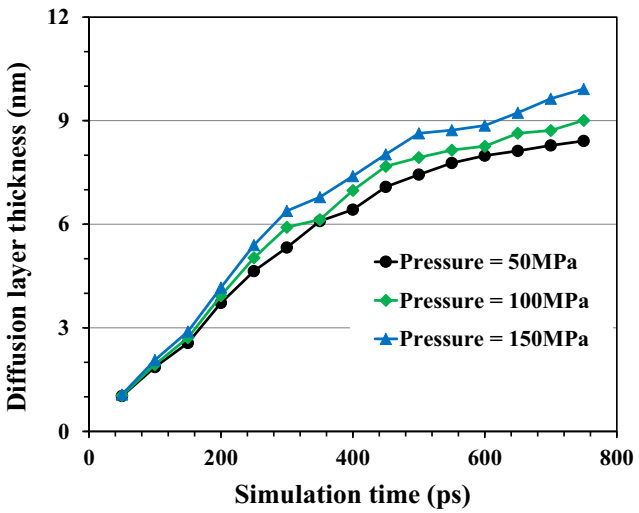

Fig. 9 Evolution of diffusion layer thickness at different interface pressure

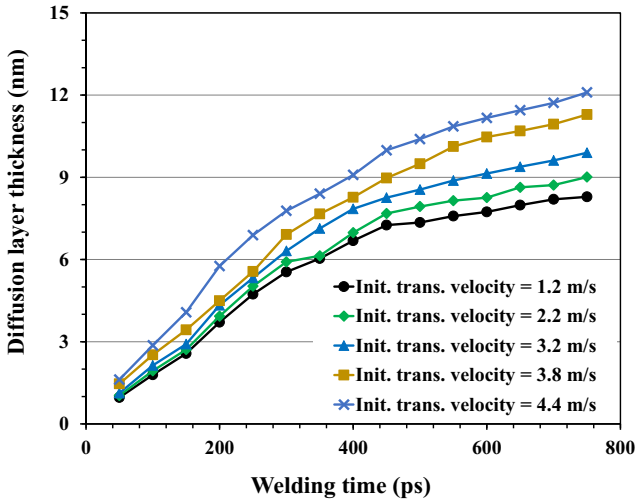

Fig. 10 Evolution of diffusion layer thickness during simulation with different initial transverse velocities

vibration increased from 1.25 to 4.4 m/s, the thickness was increased from 8 to 12 nm. Each velocity is corresponding to the velocity profile change in one-quarter of an ultrasonic vibration cycle. The conclusion coincides with higher welding energy resulting in a thicker diffusion layer.

3.2.3 Effects of material crystal structure on diffusion bonding

A few other MD simulations were conducted to conclude that the mismatched crystal orientations at the welding interface had no significant effect on diffusion layers. However,

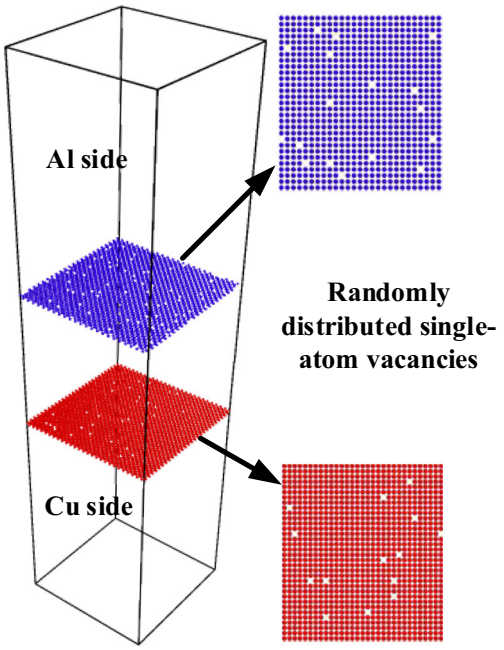

Fig. 11 MD simulation configuration showing single-atom vacancies on both Al and Cu blocks

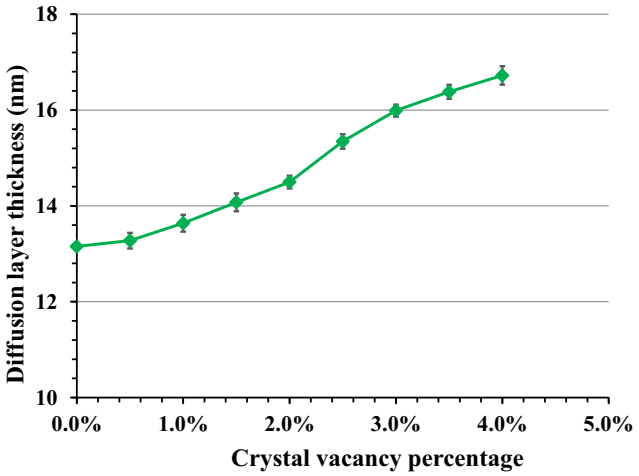

Fig. 12 Change of diffusion layer thickness as a function of crystal vacancy

vacancy defects, i.e., defects resulting from missing atoms in the crystal, were likely candidates to influence the diffusion process significantly. It has been reported that vacancy defects had a significant effect on material properties [44]. In his paper, we only considered one-atom vacancies, in which only one atom was missing. A three-dimensional (3D) random field model [45] was used to generate randomly distributed vacancies in the MD initial configuration based on a prescribed percentage of vacancy volume fraction. A schematic representation of the simulation domain with randomly distributed vacancies is shown in Fig. 11. For each prescribed vacancy volume fraction, multiple initial configurations were generated for MD simulations to consider the location uncertainty of vacancies.

Figure 12 showed the variation in diffusion layer thickness when the Al and Cu crystal blocks had vacancy volume fraction in a range of 0 to 4%. With 4% of vacancy defect, the average diffusion layer thickness can increase by 27%. When a vacancy defect exists in a crystal, neighboring atoms

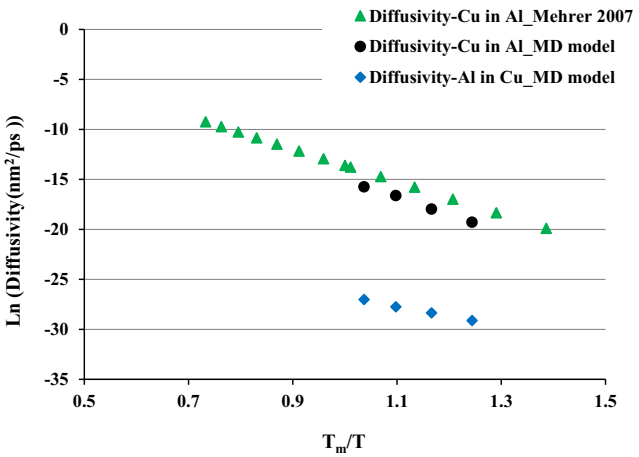

Fig. 13 Diffusivities calculation and validation

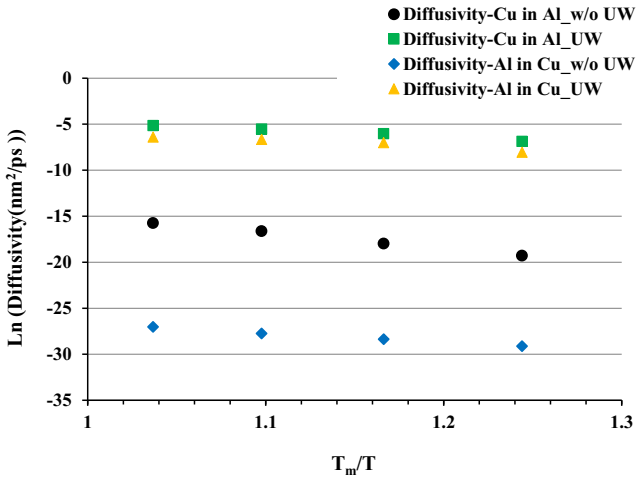

Fig. 14 Comparison of solid-state mass diffusivity for Cu in Al and Al in Cu medium at different temperatures using ultrasonic transverse velocity and without ultrasonic transverse velocity

become less stable and tend to move away from their pristine positions. The mobility of the interface atoms increased with the presence of vacancy defect. It can be concluded that more vacancy defects resulted in easier diffusion of atoms.

3.3 Hierarchical multiscale calculation

3.3.1 Diffusivity calculation via molecular dynamics

To validate the MD calculation of diffusivity, various temperatures between 750 and 900 K were considered, and the results were compared to the reported diffusivities [41]. The MD simulations were conducted under the atmospheric pressure in all directions. The diffusivity of Cu in Al was calculated at each temperature using Eq. (1). The experimentally measured diffusivities, as the baseline, were reported by Mehrer [41]. Figure 13 shows that the calculated diffusivities of Cu in Al agreed well with the experimentally reported values. Here, T_m stands for the melting temperature of Al which is considered as 933 K. As the temperature increased, the diffusivity also increased. It shall be noted that the diffusivity of Al in Cu was also calculated. It can be seen that the diffusivities of Al in Cu were significantly lower than the diffusivities of Cu in Al. It is because that Cu atoms have a smaller radius (1.278 Å) than Al atoms (1.443 Å) and Al has a larger lattice constant (4.05 Å) than Cu (3.615 Å). Therefore, it was easier for Cu atoms to diffuse into a region of Al atoms.

To calculate the Al-Cu diffusion layer thickness via the proposed hierarchical multiscale method, the diffusivity of Al in Cu and Cu in Al under the UW process needs to be calculated first via MD simulation. As a difference from the validation described above, a transverse velocity of 2.2 m/s is applied on the Al layer to initiate the relative mechanical movement according to the ultrasonic vibration. The diffusivities of both Al and Cu increased significantly as shown in Fig. 14.

We also studied the effects of the interface pressure and the initial transverse velocity on material diffusivity during the UW process as shown in Fig. 15. It can be seen that the diffusivity increased as interface pressure is increased. In addition, a higher initial transverse velocity resulted in a larger diffusivity. It is obvious that the transverse velocity encourages shear deformation and helps breakup of the regular crystal lattice. As a result, diffusion activation energy increases and more atoms diffuse across the interface. The above conclusions agree with the observation/conclusions from MD simulations of diffusion discussed in "Section 3.2."

3.3.2 Calculation for diffusion layer thickness

After obtaining the diffusivities from MD simulations, the diffusion layer thickness can be calculated via the classical

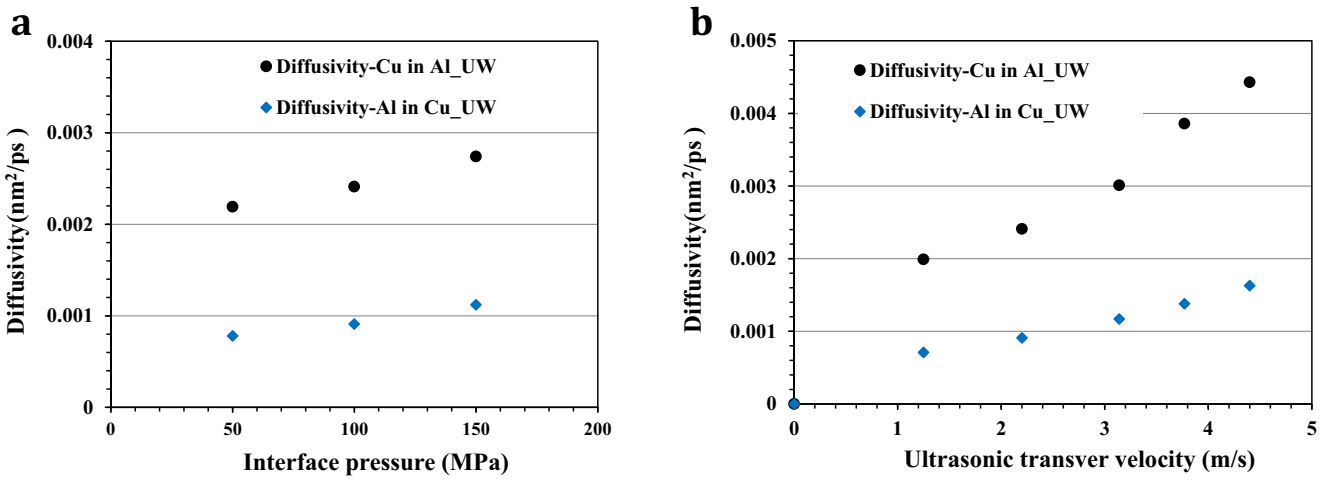

Fig. 15 **a** Diffusivity of Cu and Al at different interface pressure and **b** diffusivity of Cu and Al at different initial ultrasonic transverse velocities

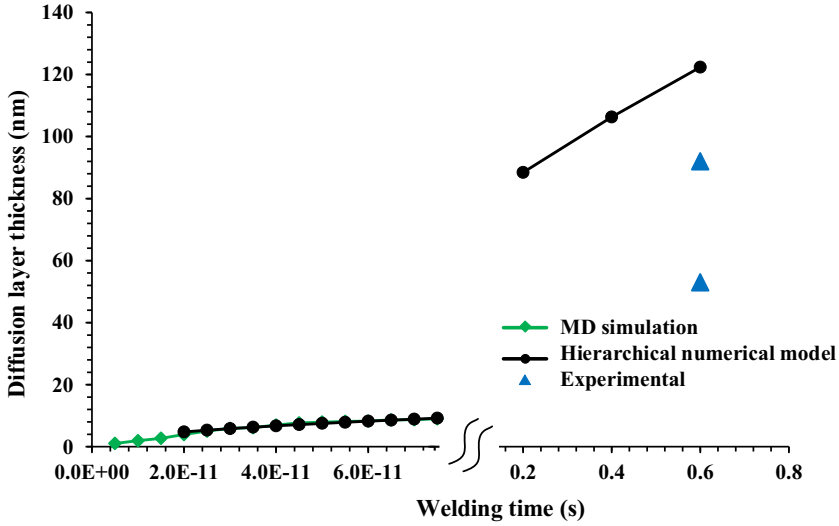

Fig. 16 Comparison of diffusion layer thickness measured from the MD model in LAMMPS and hierarchical numerical model with MD simulation and classical diffusion model and experimental measurement

diffusion model using Eq. 5. The welding time in experiments is 0.6 s since the UW process requires 0.6~1.0 s to have a good joint [3, 13]. Therefore, the MD simulation was unable to reproduce the diffusion layer thickness measured in the experiments. It has been reported that the temperature of the interface increased to a peak value during the process and went down thereafter [46, 47] during the UW process. Although the whole welding process cannot be considered as an isothermal process at the macroscale, the assumption of a constant diffusivity is adopted in the classical diffusion theory. Therefore, the diffusivity calculated from an isothermal MD simulation can be passed from the molecular model to the continuum model in the hierarchical multiscale framework.

Figure 16 compares the diffusion layer thicknesses from both MD simulations and hierarchical multiscale calculations when the welding time is in the order of a picosecond. It can be seen that the thicknesses from both methods are in a good agreement in picosecond timescale. For the MD calculation, interface temperature is used as 800 K, 100 MPa vertical interface pressure is used, and a 2.2 m/s transverse ultrasonic velocity is used. In addition, the diffusional layer thickness is also predicted by the hierarchical multiscale approach at the actual welding timescale. The predicted diffusion layer thickness is 122 nm, which is overpredicted compared to experimentally measured thickness. In the MD simulation, the starting interface is considered as an ideal condition with no surface peak and valleys whereas, during actual experiments, the surface processes surface roughness. At the same time, there is local pressure difference at the peak and valley of the interfacial region which also contributes to the wide variation of diffusion layer thickness during experiments. However, during the MD simulation, only one pressure condition is considered at the interface. Considering all those assumptions to simplify the MD model, the predicted final diffusion layer thickness agrees well to the experimental result.

4 Conclusions

In this paper, a comprehensive review is conducted on the diffusion bonding phenomena during the UW process and the process variables that influence the diffusion process. An atomistic simulation was used to investigate the interface diffusion during the UW process of dissimilar material (Al and Cu). A molecular dynamics model was developed for the first time that considered the effect of transverse ultrasonic vibration to simulate the evolution of the diffusion layer during the UW process. The classical diffusion theory and MD simulations were combined into a hierarchical multiscale model to calculate the thickness of the diffusion layer during the process. The influence of transverse ultrasonic velocity on the atom diffusion at the atomic level is approximated by thermal energy at the interface and mechanical movement of atoms. The solid-state diffusivity was calculated from the MD simulation result. Numerical time integration was performed on the diffusivity value at different positions within an ultrasonic vibration cycle to incorporate the effect of a complete sinusoidal vibration cycle. The proposed model is capable to predict the diffusion behavior and its dependence on process variables. The effects of randomly located vacancy defects on the diffusion layer thickness were also investigated in the study. The vacancy defect helped to increase the mobility of the atoms to diffuse deeper into the opposite crystal resulting in an increase of diffusion thickness. This model provides a guideline to control the diffusion phenomena and the diffusion layer thickness during the UW process.

Funding information The authors would like to the financial support of the National Science Foundation under Grant Number CMMI-1537512.

References

1. Kazuhiro N, Masao U (2002) Needs and prospects of dissimilar metal joining and welding. J Japan Weld Soc 71:418–421. https://doi.org/10.2207/qjjws1943.71.418
2. Martinsen K, Hu SJ, Carlson BE (2015) Joining of dissimilar materials. CIRP Ann - Manuf Technol 64:679–699. https://doi.org/10.1016/j.cirp.2015.05.006
3. Lee SS, Kim T-H, Hu SJ et al (2013) Characterization of joint quality in ultrasonic welding of battery tabs. ASME J Manuf Sci Eng 135:021004. https://doi.org/10.1115/1.4023364
4. Kicukov E, Gursel A (2015) Ultrasonic welding of dissimilar materials: a review. Period Eng Nat Sci 3:28–36. https://doi.org/10.21533/pen.v3i1.44
5. Li J, Han L, Zhong J (2008) Short-circuit diffusion of ultrasonic bonding interfaces in microelectronic packaging. Surf Interface Anal 40:953–957. https://doi.org/10.1002/sia.2840
6. Zhao YY, Li D, Zhang YS (2013) Effect of welding energy on interface zone of Al–Cu ultrasonic welded joint. Sci Technol Weld Join 18:354–360. https://doi.org/10.1179/1362171813Y.0000000114
7. Wu X, Liu T, Cai W (2015) Microstructure, welding mechanism, and failure of Al/Cu ultrasonic welds. SME J Manuf Process 20:321–331. https://doi.org/10.1016/j.jmapro.2015.06.002
8. Yang Y, Janaki Ram GD, Stucker BE (2009) Bond formation and fiber embedment during ultrasonic consolidation. J Mater Process Technol 209:4915–4924. https://doi.org/10.1016/j.jmatprotec.2009.01.014
9. Ginzburg S, Mitskevich A, Nosov Y (1967) Formation of the joint in ultrasonic welding. Weld Prod 13:45–47
10. Chang UI, Frisch J (1974) On optimization of some parameters in ultrasonic metal welding. Weld J 53:24–35
11. Lu Y, Song H, Taber GA, Foster DR, Daehn GS, Zhang W (2016) In-situ measurement of relative motion during ultrasonic spot welding of aluminum alloy using photonic Doppler velocimetry. J Mater Process Technol 231:431–440. https://doi.org/10.1016/j.jmatprotec.2016.01.006
12. Fujii HT, Goto Y, Sato YS, Kokawa H (2016) Microstructure and lap shear strength of the weld interface in ultrasonic welding of Al alloy to stainless steel. Scr Mater 116:135–138. https://doi.org/10.1016/j.scriptamat.2016.02.004
13. Zhang Z, Wang K, Li J, Yu Q, Cai W (2017) Investigation of interfacial layer for ultrasonic spot welded aluminum to copper joints. Sci Rep 7:12505. https://doi.org/10.1038/s41598-017-12164-2
14. Yang JW, Cao B, He XC, Luo HS (2014) Microstructure evolution and mechanical properties of Cu–Al joints by ultrasonic welding. Sci Technol Weld Join 19:500–504. https://doi.org/10.1179/1362171814Y.0000000218
15. Beyer W (1969) The bonding process in the ultrasonic welding of metals. Schweisstechnik 19:16–20
16. Watanabe T, Sakuyama H, Yanagisawa A (2009) Ultrasonic welding between mild steel sheet and Al–Mg alloy sheet. J Mater Process Technol 209:5475–5480. https://doi.org/10.1016/j.jmatprotec.2009.05.006
17. Watanabe A, Yanagisawa T, Konuma S et al (1999) The effect of oxide film on the strength of an ultrasonically welded joint and welding process - study of the ultrasonic welding of dissimilar metals (2nd report). Weld Int 13:936–944. https://doi.org/10.1080/09507119909452077
18. Xu L, Wang L, Chen Y-C, Robson JD, Prangnell PB (2016) Effect of interfacial reaction on the mechanical performance of steel to aluminum dissimilar ultrasonic spot welds. Metall Mater Trans A 47:334–346. https://doi.org/10.1007/s11661-015-3179-7
19. Ren D, Zhao K, Pan M, Chang Y, Gang S, Zhao D (2017) Ultrasonic spot welding of magnesium alloy to titanium alloy. Scr Mater 126:58–62. https://doi.org/10.1016/j.scriptamat.2016.08.003
20. Mielke SL, Troya D, Zhang S, Li JL, Xiao S, Car R, Ruoff RS, Schatz GC, Belytschko T (2004) The role of vacancy defects and holes in the fracture of carbon nanotubes. Chem Phys Lett 390:413–420. https://doi.org/10.1016/j.cplett.2004.04.054
21. Xiao S, Hou W (2006) Fracture of vacancy-defected carbon nanotubes and their embedded nanocomposites. Phys Rev B Condens Matter Mater Phys 73:1–7. https://doi.org/10.1103/PhysRevB.73.115406
22. Xiao S, Andersen DR, Han R, Hou W (2006) Studies of carbon nanotube-based oscillators using molecular dynamics. J Comput Theor Nanosci 3:142–147. https://doi.org/10.1166/jctn.2006.013
23. Xiao S, Hou W (2007) Studies of nanotube-based resonant oscillators through multiscale modeling and simulation. Phys Rev B Condens Matter Mater Phys 75:1–9. https://doi.org/10.1103/PhysRevB.75.125414
24. Ghaffari MA, Zhang Y, Xiao SP (2017) Molecular dynamics modeling and simulation of lubricant between sliding solids. J Micromechanics Mol Phys 2:1750009. https://doi.org/10.1142/S2424913017500096
25. Chen SY, Wu ZW, Liu KX, Li XJ, Luo N, Lu GX (2013) Atomic diffusion behavior in Cu-Al explosive welding process. J Appl Phys 113:044901. https://doi.org/10.1063/1.4775788
26. Konovalenko IS, Konovalenko IS, Psakhie SG (2017) Molecular dynamics modeling of bonding two materials by atomic scale friction stir welding. 020093:020092. https://doi.org/10.1063/1.5013773
27. Ye YY, Biswas R, Morris JR, Bastawros A, Chandra A (2003) Molecular dynamics simulation of nanoscale machining of copper. Nanotechnology 14:390–396. https://doi.org/10.1088/0957-4484/14/3/307
28. Li C, Li D, Tao X, Chen H, Ouyang Y (2014) Molecular dynamics simulation of diffusion bonding of Al–Cu interface. Model Simul Mater Sci Eng 22:065013. https://doi.org/10.1088/0965-0393/22/6/065013
29. Chen SD, Soh AK, Ke FJ (2005) Molecular dynamics modeling of diffusion bonding. Scr Mater 52:1135–1140. https://doi.org/10.1016/j.scriptamat.2005.02.004
30. Chen S, Ke F, Zhou M, Bai Y (2007) Atomistic investigation of the effects of temperature and surface roughness on diffusion bonding between Cu and Al. Acta Mater 55:3169–3175. https://doi.org/10.1016/j.actamat.2006.12.040
31. Zhang Q, Lai WS, Liu BX (1999) Molecular dynamics study of solid state interfacial reaction in the Ni-Mo system. J Comput Mater Des 6:103–116. https://doi.org/10.1023/A:100874620
32. Lee SS, Kim T-H, Hu SJ et al (2015) Analysis of weld formation in multilayer ultrasonic metal welding using high-speed images. ASME J Manuf Sci Eng 137:031016. https://doi.org/10.1115/1.4029787
33. Shen N (2018) Microstructure prediction of severe plastic deformation manufacturing processes for metals. University of Iowa
34. Shen N, Samanta A, Ding H, Cai WW (2016) Simulating microstructure evolution of battery tabs during ultrasonic welding. SME J Manuf Process 23:306–314. https://doi.org/10.1016/j.jmapro.2016.04.005
35. Zhao J, Li H, Choi H, Cai W, Abell JA, Li X (2013) Insertable thin film thermocouples for in situ transient temperature monitoring in ultrasonic metal welding of battery tabs. SME J Manuf Process 15:136–140. https://doi.org/10.1016/j.jmapro.2012.10.002
36. Plimpton S (1995) Fast parallel algorithms for short-range molecular dynamics. J Comput Phys 117:1–19. https://doi.org/10.1006/jcph.1995.1039

37. Cai J, Ye YY (1996) Simple analytical embedded-atom-potential model including a long-range force for fcc metals and their alloys. Phys Rev B 54:8398–8410. https://doi.org/10.1103/PhysRevB.54.8398
38. Nose S (1984) A unified formulation of the constant temperature molecular dynamics methods. J Chem Phys 81:511–519. https://doi.org/10.1063/1.447334
39. Hoover WG (1985) Canonical dynamics: equilibrium phase-space distributions. Phys Rev A 31:1695–1697. https://doi.org/10.1103/PhysRevA.31.1695
40. Parrinello M, Rahman A, R a PM (1980) Crystal structure and pair potentials: a molecular-dynamics study. Phys Rev Lett 45:1196–1199. https://doi.org/10.1103/PhysRevLett.45.1196
41. Mehrer H (2007) Diffusion in solids: fundamentals, methods, materials, diffusion-controlled processes. Springer, Berlin Heidelberg
42. Taneja D, Volpert M, Hodaj F (2018) On the initial stages of solid state reactions in Ni/Sn-Ag solder system at 150–210 °C. J Alloys Compd 742:199–211. https://doi.org/10.1016/j.jallcom.2018.01.253
43. Bai L, Xue W, Li Y, Liu X, Li Y, Sun J (2018) The interfacial behaviours of all-solid-state lithium ion batteries. Ceram Int 44:7319–7328. https://doi.org/10.1016/j.ceramint.2018.01.190
44. Hou W, Xiao S (2007) Mechanical behaviors of carbon nanotubes with randomly located vacancy defects. J Nanosci Nanotechnol 7:4478–4485. https://doi.org/10.1166/jnn.2007.862
45. Soyarslan C, Bargmann S, Pradas M, Weissmüller J (2018) 3D stochastic bicontinuous microstructures: generation, topology and elasticity. Acta Mater 149:326–340. https://doi.org/10.1016/j.actamat.2018.01.005
46. Li H, Choi H, Ma C, Zhao J, Jiang H, Cai W, Abell JA, Li X (2013) Transient temperature and heat flux measurement in ultrasonic joining of battery tabs using thin-film microsensors. ASME J Manuf Sci Eng 135:051015. https://doi.org/10.1115/1.4024816
47. Chen KK, Zhang YS (2015) Numerical analysis of temperature distribution during ultrasonic welding process for dissimilar automotive alloys. Sci Technol Weld Join 20:522–531. https://doi.org/10.1179/1362171815Y.0000000022